DEFINING DYNAMIC ROUTE STRUCTURE FOR AIRSPACE CONFIGURATION

Shannon Zelinski, Michael Jastrzebski
NASA Ames Research Center, University of California Santa Cruz

Keywords: *airspace configuration, traffic flow, critical points, routing*

Abstract

This paper describes a method for defining route structure from flight tracks. Dynamically generated route structures could be useful in guiding dynamic airspace configuration and helping controllers retain situational awareness under dynamically changing traffic conditions. Individual merge and diverge intersections between pairs of flights are identified, clustered, and grouped into nodes of a route structure network. Links are placed between nodes to represent major traffic flows. A parametric analysis determined the algorithm input parameters producing route structures of current day flight plans that are closest to todays airway structure. These parameters are then used to define and analyze the dynamic route structure over the course of a day for current day flight paths. Route structures are also compared between current day flight paths and more user preferred paths such as great circle and weather avoidance routing.

Nomenclature

A	=	airway structure
B	=	boundary
C	=	cluster
D	=	diverge
I	=	intersection
L	=	link
M	=	merge
N	=	node
n	=	number
P	=	path or sequence of points
p	=	point position
R	=	route structure
r	=	lateral radial distance
S	=	airway segment
w	=	weight
z	=	vertical distance
δ	=	structure deviation
η	=	boundary proximity percentage
λ	=	structure representation
ρ	=	intersection representation
σ	=	standard deviation
τ	=	flight track data time range
ω	=	filtering threshold

1 Introduction

The current airspace sector design evolved over decades, driven by human-centered separation assurance and an airway system of ground-based navaids. The future system is migrating toward more direct and flexible user-preferred routing. Automation tools and dynamic reconfiguration of airspace boundaries will enable controllers

to adapt to changing weather and traffic conditions and increase controller staffing flexibility. Structure-based abstractions of traffic conditions are necessary both to trigger and guide airspace boundary changes and to quickly give controllers situational awareness. Histon et al [1] identified elements of structure-based traffic abstraction that controllers use to maintain airspace situation awareness. Two key elements identified, standard flows and critical points (where major flows cross and merge), have been used as inputs in several automated airspace boundary reconfiguration methods [2, 3, 4, 5]. Complex air traffic networks have been developed to study aggregate system behavior and robustness to disturbances [6]. Route structure is an abstraction of the air traffic network based on standard flows and critical points. A method of quickly determining route structure is necessary for controllers and airspace configuration to adjust to flexible user-preferred routing.

Several methods have been proposed to define the route structure elements of a given set of flight trajectories. Most methods begin with two-dimentional grid structures that capture information about traffic passing through each grid cell. Xue [3] used the heading variance of flights within each grid cell to determine if the cell belonged to a major traffic flow or intersection point and could be used as an airspace boundary constraint. Other methods used flight occupancy counts within each grid cell along with other techniques to bundle flight trajectories into flows [7] or to create an abstract network flow graph of traffic [4]. Of the methods that defined route structure connections between flows and critical points, Sabhnani et al [7] proposed two top-down approaches that first identified flows and then defined their intersections to be critical points, whereas work preceding this paper [8] proposed a bottom-up approach that identified critical points first. Li et al [5] took a short cut by refining a complex route structure generated from flight plans. However, this approach depended upon the existing airway structure elements found in today's flight plans.

This paper extends preceding work [8] by adding an altitude component to critical point identification and linking critical points together with flows to form a route structure. A parametric analysis is performed to determine the algorithm input parameters that produce route structures that are closest to today's airway structure. These parameters are then used to extract and analyze the dynamic changing route structure over the course of a day for current day flight paths and for more user preferred paths such as great circle and weather avoidance routing.

The remainder of this paper is organized as follows. Section 2 describes the method of defining route structure from flight tracks. A parametric analysis identifies optimal method parameters in section 3. Sections 4 and 5 analyze route structures from dynamically shifting time windows of traffic, and from alternate user preferred routing, respectively. Finally, conclusions are presented in section 6.

2 Defining Route Structure

This section describes how flight track data are processed to define a route structure. First individual intersection points were generated from pairs of flights within lateral and vertical proximity of one another. Intersection points within another set of specified lateral and vertical proximity of one another formed cluster points. Clusters were further grouped into nodes to simplify the structure. Finally, links were placed between nodes with the nominal paths of flights forming each link representing flow paths.

2.1 Proximate Points

The first step in route structure generation identifies points on pairs of flight tracks that come within a specified proximity of one another. Let $P = p_1, ..., p_n$ be an ordered set of latitude/longitude/altitude/time coordinates describing the trajectory of flight P. Similarly, let $Q = q_1, ..., q_m$ describe the trajectory of flight Q. For all points within a specified time range, any point in P that comes within a lateral radius r_I and vertical distance z_I of any point in Q is a proximate

point of P with respect to Q.

2.2 Intersections

Merge and diverge intersections classify the interactions between pairs of flights. When two flights come within a specified proximity of one another, their paths merge. When two flights originally within a specified proximity of one another are no longer within the specified proximity, their paths diverge. For every consecutive sequence of flight track coordinates on P that are proximate to Q, the first point is a merge intersection, and the last point is a diverge intersection. For every intersection on P with respect to Q, an intersection is also identified on Q with respect to P.

Boundary intersections occur where flights cross a given airspace boundary. Any two consecutive points on a flight track that are in different specified airspace regions, such as sectors or centers, produce boundary intersections. These are not necessary to generate a route structure. However, if a route structure is generated for only a specified bounded region, boundary intersections make it possible to identify flows that enter or exit the region.

Rather than storing single instances of intersection, flight track points are tagged as merge and diverge intersections with respect to multiple other flights and as boundary intersections when straddling a boundary. Each flight track point tagged with merges defines a merge intersection I_{Mi} with position $p(I_{Mi})$ identical to the track point position and with weight $w(I_{Mi})$ equal to the number of individual merges identified with respect to other flights at this track point. A diverge intersection I_{Di} is defined similarly. A boundary intersection I_{Bi} is different only in that $w(I_{Bi}) \equiv 1$ because a single track point cannot intersect the same boundary multiple times. This method allows a single flight track point to define up to three intersections, one of each type.

2.3 Clusters

Clusters characterize groups of intersections within close spacial proximity. Each intersection may belong to only one cluster in an intersection to cluster ($I \rightarrow C$) mapping. The position $p(C_i)$ and weight $w(C_i)$ of cluster C_i are the centroid and sum weight of the intersections within C_i, respectively. Sets I_M, I_D, and I_B are clustered separately to form sets of merge clusters, $C_M = \{C_{M1}, C_{M2}, ...\}$, diverge clusters, $C_D = \{C_{D1}, C_{D2}, ...\}$, and boundary clusters, $C_B = \{C_{B1}, C_{B2}, ...\}$, respectively.

An agglomerative clustering technique was used because it handles data outliers well and automatically determines the final number of clusters. Pairs of intersection points are clustered in order of increasing lateral distance if they are within r_C and z_C of each other. Each grouped point pair is replaced by the group centroid for consideration in the next clustering iteration. The process repeats until all groups with centroids within r_C and z_C of each other are clustered. Boundary intersections are different enough from merge and diverge intersections, that unique clustering parameters, r_{C_B} and z_{C_B}, are used to cluster boundary intersections.

The resulting set of clusters may contain numerous low weight outliers, caused by random traffic, which should be filtered. A different weight threshold should be used for filtering different time ranges of flight track data analyzed. Let τ be the flight track data time range and let ω_C be a rate threshold such that cluster C_i is filtered if $w(C_i) < \tau \cdot \omega_C$. This way, the same ω_C may be used for various τ with similar filtering effect. Because boundary cluster weights are determined by instances of flights crossing a boundary rather than instances of flight pair intersections, a unique ω_{C_B} filters boundary clusters.

2.4 Nodes

Nodes are at the top level of intersection groupings and serve as the end points for links representing traffic flows. Crossing traffic flows may form merge and diverge clusters very close to one another or merge or diverge clusters may exist very close to the boundary. Therefore, nodes are used to represent groups of clusters of mixed type. Building a network of flows between nodes

rather than individual clusters significantly simplifies and strengthens the resulting route structure.

Each cluster may belong to only one node. A boundary node refers to any node containing a boundary cluster. Interior nodes refer to nodes without any boundary clusters. The position $p(N_i)$ of node N_i is the centroid of all clusters within N_i. Node weight $w(N_i)$ is the sum weight of all clusters within N_i. Nodes can also be expressed as groups of intersections belonging to its clusters ($I \rightarrow C \rightarrow N \equiv I \rightarrow N$). The spacial size of node N_i is measured by the three dimensional standard deviation, $\sigma(N_i) = (\sigma_x(N_i), \sigma_y(N_i), \sigma_z(N_i))$, of all I within N_i from $p(N_i)$.

A different method is used to group clusters into nodes than intersections into clusters. Initially each cluster defines a unique node. Nodes with overlapping σ are too close with respect to their spacial size to serve as traffic flow end points. Therefore, if the distances between nodes $d(N_i, N_j) < \sigma(N_i) + \sigma(N_j)$ in all three dimensions, then clusters within N_i and N_j are grouped into a single node. Additionally, if a single track point defines multiple intersections grouped to unique nodes, these nodes are grouped into a single node.

2.5 Links

Links are directed connections between pairs of nodes representing traffic flow. Through $I \rightarrow N$ mappings, all flights with track points defining intersections, may be expressed as a sequence of nodes along the flight trajectory. Let L_{ij} specify a set of flight segments from N_i to N_j. Only segments between consecutive nodes along a flight trajectory are considered. Let link weight $w(L_{ij})$ be the number of flight segments in L_{ij}. Let $P(L_{ij})$ specify the nominal path or flow path of all segments in L_{ij}. Link paths may curve and bend around special use airspace or weather as they travel between nodes. The sample rate used to define link paths is one point every 8 nmi. This sample rate is similar in distance to the 1-minute resolution flight tracks analyzed.

As with clusters, the resulting set of links may have many low weight outliers which should be filtered. Let ω_L be a rate threshold such that link L_{ij} is filtered if $w(L_{ij}) < \tau \cdot \omega_L$. Filtering links also has an additional filtering effect on nodes. Boundary nodes with less than one link and interior nodes with less than two links are filtered. If nodes are filtered, links are recalculated and the process iterates until the number of nodes and links stabilizes.

3 Parametric Analysis

There are a number of parameters described in section 2 that affect the fidelity of the resulting route structure. Route structure links and nodes are functionally equivalent to today's airways and their intersections. Results from a range of parameters are analyzed to find values that produce route structure similar to today's airway structure.

Flight tracks used to generate the route structures were 1-minute resolution simulated trajectories of flight schedules and filed flight plans from a high traffic volume, good weather Tuesday on 4/21/2009. This analysis focused on high altitude tracks in Kansas City Center (ZKC) during the peak four hours, approximately 15:30-19:30 ZKC local time. Because the ZKC high altitude sector floor was 24,000 ft, only tracks at 24,000 ft and above were considered.

There are four types of airways in the US. V-routes (below 18,000 ft) and J-routes (above 18,000 ft) are classic airways using ground-based navaids. T-routes (below 18,000 ft) and Q-routes (above 18,000 ft) are newer area navigation or RNAV-based airways. This analysis focused on the 38 J-routes and 2 Q-routes in high altitude ZKC shown in Fig. 1.

3.1 Parameters

There are three types of parameters used to define route structure. The parameters used to define intersection points are r_I and z_I. The parameters used to define cluster points are r_C, z_C, r_{C_B}, and z_{C_B}. Finally, parameters ω_C, ω_{C_B}, and ω_L

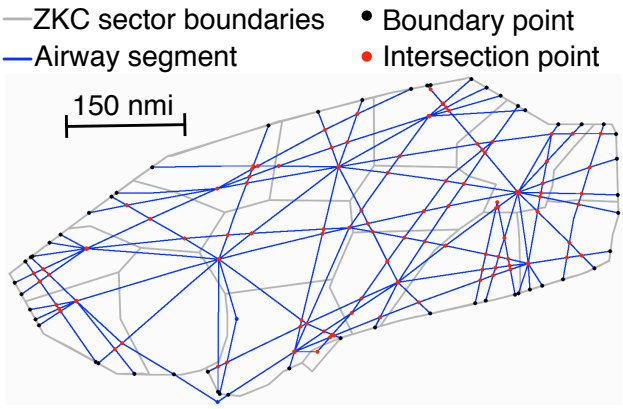

Fig. 1 Airways and their intersections within high altitude Kansas City Center (ZKC).

filter low weight clusters and links. The range of intersection and cluster parameters explored was designed with aircraft separation tolerances in mind. En-route lateral and vertical aircraft separation tolerances are five nmi and 1,000 ft, respectively. Therefore, the analysis considered values of r_I, r_C, and r_{C_B} between three and 30 nmi and values of z_I, z_C, and z_{C_B} between 500 and 3,000 ft. Recall from section 2 that each flight pair interaction produces two intersection points, one on each flight trajectory, separated by as much as r_I laterally and z_I vertically. Therefore, $r_C \geq r_I$ and $z_C \geq z_I$ to guarantee that these points are clustered. Filtering parameters were increased from zero.

3.2 Route Structure Evaluation

Route structure results from each set of parameters were evaluated to determine their precision and accuracy. Precision metrics compare route structure to the individual flight tracks they represent and accuracy metrics compare route structure to the current airway structure.

Precision metrics include traffic deviations from route structure and route structure intersection representation. Let $\sigma_r(L_{ij})$ be the lateral standard deviation, of all flight track segments in L_{ij} from $P(L_{ij})$. Let traffic deviation $\sigma_r(L)$ be the average of all $\sigma_r(L_{ij})$ weighted by $w(L_{ij})$.

Route structure intersection representation, ρ, measures the ratio of flight intersections represented by the final route structure. It is the ratio of sum weight of all nodes over the sum weight of all intersections before cluster filtering. If all filtering parameters were zero, ρ would always be one.

Route structure accuracy metrics compare route structure with airway structure to find the right balance of abstraction and precision. Let S_{ij} specify the airway segment between airway intersections M_i and M_j. Just as link nominal path points are positioned every eight nmi along each path, airway path points are placed every eight nmi along each airway segment. Let $P(S_{ij})$ be the sequence of (x,y) points every eight nmi along S_{ij}. Unlike links, airway segments do not have a vertical component or a weight.

Accuracy metrics include deviation and representation metrics between airway and route structure. The route structure deviation, δ_R, is the average lateral distance of each link nominal path point $p_k(L_{ij})$ from its closest airway segment, weighted by $w(L_{ij})$. The airway structure deviation, δ_A, is the average lateral distance of each airway path point $p_k(S_{ij})$ from it's closest link.

Airway and route structure representations are the ratios of each structure found to be closest to a piece of the other structure. Let $n_{S_{ij}}$ be the number of path points on $P(S_{ij})$. Let $n_{L(S_{ij})}$ be the number of points from all $P(L)$ identifying S_{ij} as the closest airway segment. The airway structure representation is defined as

$$\lambda_A = \frac{\sum \min[n_{S_{ij}}, n_{L(S_{ij})}]}{\sum n_{S_{ij}}}.$$

Similarly, let $n_{L_{ij}}$ be the number of path points on $P(L_{ij})$ and let $n_{S(L_{ij})}$ be the number of points from all $P(S)$ identifying L_{ij} as the closest link. The route structure representation is defined as

$$\lambda_R = \frac{\sum [\min[n_{L_{ij}}, n_{S(L_{ij})}] \cdot w(L_{ij})]}{\sum [n_{L_{ij}} \cdot w(L_{ij})]}.$$

This is similar to λ_A calculation, only λ_R is weighted by $w(L_{ij})$.

Table 1 summarizes the precision and accuracy metrics. The right column indicates the goal of the parametric analysis to either minimize (-) or maximize (+) each metric. Note that the goal is to minimize all deviation metrics and maximize all representation metrics.

Table 1 Summary of route structure evaluation metrics

Precision Metrics			
$\sigma_r(L)$	=	lateral traffic deviation	-
ρ	=	intersection representation	+

Accuracy Metrics			
δ_R	=	route structure deviation	-
δ_A	=	airway structure deviation	-
λ_R	=	route structure representation	+
λ_A	=	airway structure representation	+

3.3 Results

The goal of the parametric analysis was to find parameters that minimized σ and δ metrics, and maximized ρ and λ metrics. A simple optimization formula was designed to combine the metrics in Table 1 into a single value to minimize by multiplying metrics to minimize and dividing by metrics to maximize.

$$J = \frac{\sigma_r(L) \cdot \delta_R \cdot \delta_A}{\rho \cdot \lambda_R \cdot \lambda_A}$$

This function was used to guide the search for route structure parameters that produced the smallest deviation metrics with the largest and most balanced structure representation metrics. Balanced structure representation metrics ensured that the airway and route structure network lengths were similar and thus represented traffic at a similar level of abstraction.

Table 2 shows the set of optimal parameter values identified and used in remaining route structure analyses. The optimal intersection parameters were very similar to standard separation criteria with r_I equalling the lateral standard and z_I only 200 ft greater than the vertical standard. As expected, all clustering parameters were greater than intersection parameters. Boundary intersection clustering required a r_{C_B} almost three times r_C. Merge and diverge clustering produced much larger weight clusters than boundary intersection clustering. Therefore, ω_C is eight times larger than ω_{C_B}. Links were less seldom formed due to the requirement of full flight trajectory segments between nodes and because they were iteratively filtered. Therefore, ω_L was never raised above one.

Table 2 Optimal set of route structure generation parameters.

r_I	=	5 nmi	z_I	=	1,200 ft
r_C	=	6 nmi	z_C	=	2,000 ft
r_{C_B}	=	17 nmi	z_{C_B}	=	2,000 ft
ω_C	=	20 *w*/hr	ω_{C_B}	=	2.5 *w*/hr
ω_L	=	1 *w*/hr			

Table 3 shows the evaluation metrics obtained using the parameters in Table 2. In general, $\sigma_r(L)$ responded mostly to intersection and cluster parameters. As ω_C and ω_{C_B} were increased, ρ and λ_A decreased slightly, and λ_R increased. When the filtering parameters were increased too much, ρ and λ_A began to fall more rapidly. The higher λ_A and λ_R, the lower there respective δ_A and δ_R were. This is because portions of the unrepresented structure began to skew deviation metrics with closest distances to parts of the other structure that clearly did not match. In general, δ_A tended to be greater than δ_R because many unrepresented links were in similar lateral locations as other links at different altitudes. The airway structure was more prone to skewing δ_A due to underutilized airway segments. The optimal parameters were chosen such that λ_A and λ_R were somewhat balanced and as high as possible.

Figure 2 illustrates the route structure generated from the parameters in Table 2. Links are shown as lines with color indicating link weight. Nodes are shown as red dots with size indicating node weight. Because node weight tends to increase very quickly, the square root of node weight is shown to better view relative

Table 3 Evaluation metrics obtained from optimal set of route structure generation parameters.

$\sigma_r(L)$	=	1.79 nmi	ρ	=	0.57
δ_A	=	5.81 nmi	λ_A	=	0.73
δ_R	=	1.67 nmi	λ_R	=	0.53

weights. Black and gray lines underlying the route structure are the same airway segments and sector boundaries, respectively, shown in Fig. 1. The route structure completely overlaps many of these black lines. Figure 2 visually confirms the accuracy metrics from Table 3. It can be seen that route structure elements that follow the airway structure, follow closely. Some airway segments do not get enough traffic to be represented at all whereas a few links highlight flows where no published airway segment exists. Because route structure is altitude specific, Fig. 2 shows several instances where links appear to overlap or cross without a node.

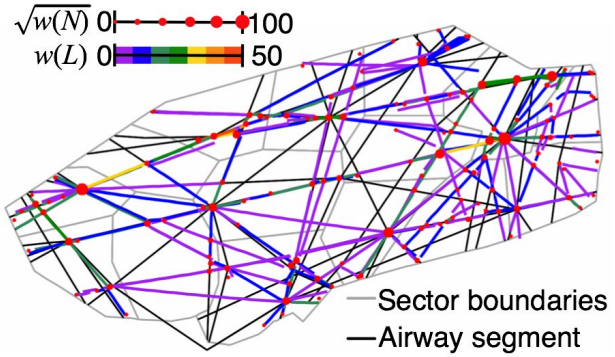

Fig. 2 Route structure generated from optimal parameters overlaying airways.

3.4 Robustness Verification

The parametric analysis calibrated route structure parameters to a single day. To demonstrate that these parameters do not need to be re-calibrated, the same parameters optimized for 4/21/2009 were used to create route structures for the peak four-hour periods of three other low-weather Tuesdays spread throughout 2009. Table 4 shows the evaluation metrics as well as a few additional metrics for all four days. Additional metrics include number of flights (n_f), number of links (n_L), number of nodes (n_N), average link weight (w_L), average node weight (w_N), and the average lateral standard deviation of points within each node from the node centroid ($\sigma_r(N)$). Metrics are grouped into numbers, average weights, representation ratios, and deviations. The values for each metric are very similar when compared between different days, nor are 4/21/2009 metrics always the best. This verifies that the chosen set of parameters are robust to different days of flight schedules. The same parameters are used to analyze dynamic route structure and route structures for user preferred routing in following sections.

Table 4 Evaluation metrics from the peak four-hour periods of four low weather Tuesdays in 2009.

	2/10	4/21	7/14	11/10
n_f	1,098	1,054	1,059	1,064
n_L	285	315	284	268
n_N	129	138	121	125
w_L	9.46	9.83	9.87	10.77
w_N	510.80	554.88	545.07	604.38
ρ	0.52	0.57	0.51	0.56
λ_A	0.73	0.73	0.75	0.72
λ_R	0.60	0.53	0.58	0.59
$\sigma_r(L)$	2.26	1.79	2.07	2.05
$\sigma_r(N)$	4.69	4.69	5.07	4.78
δ_A	4.45	5.81	5.47	4.78
δ_R	1.71	1.67	1.73	1.86

4 Dynamic Route Structure

One of the main potential benefits of route structure is that it may be generated dynamically to visualize how the structure changes with time. Figure 3 shows multiple route structures from 4/21/2009 by shifting the four-hour time window in two-hour increments from the peak four-hours shown in Fig. 2. In some instances, links and nodes move slightly, but for this good weather

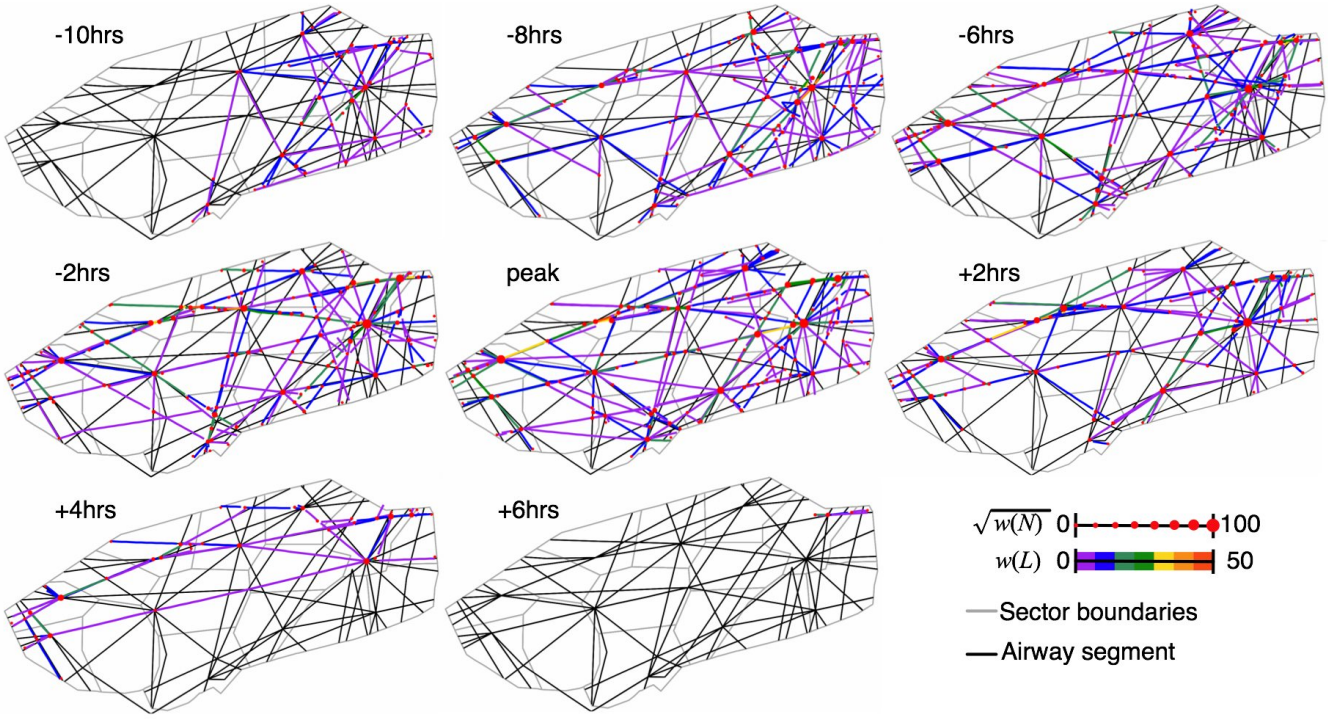

Fig. 3 Dynamic route structure shifted every two hours.

day, most of the route structure dynamics are increases and decreases in weight. Nodes and links appear and increase in weight up to the peak time period, after which they begin to decrease in weight and disappear. Tracks from time ranges outside of the peak-10 hours to peak+6 hours shown did not produce any route structure.

The numbers of flights, links, and nodes (n_f, n_L, and n_N) for each of the route structures from Fig. 3 are shown in Fig. 4. Average link and node weights (w_L and w_N) are shown in Fig. 5. Both link and node numbers and weights correlate with the number of flights, especially nodes.

Figure 6 shows intersection, airway, and route structure representations (ρ, λ_A, and λ_R) for each of the route structures from Fig. 3. Intersection and airway representations increase with number of flights, whereas route structure representation decreases. This is because as segments of the airway structure saturate, more and more flows are formed in places where no airway has been published.

Average deviation metrics are shown in Fig.

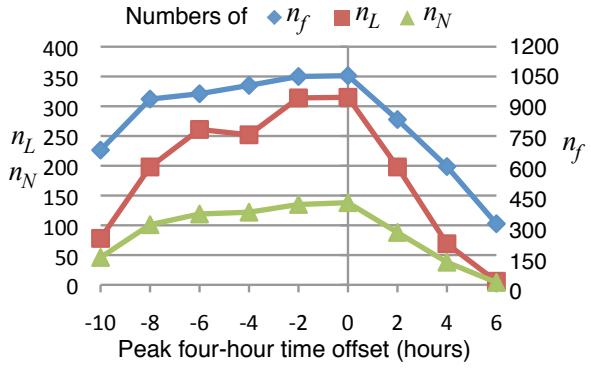

Fig. 4 Dynamic route structure shifted every two hours.

7. The average lateral standard deviations of intersection points for their node centroids ($\sigma_r(N)$) and flight tracks from their link paths ($\sigma_r(L)$) are stable with respect to number of flights. These metrics depend far more on the route structure generation parameters than the track data processed. Route structure deviation from airways is also very stable. However, airway deviation from route structure correlates heavily to route

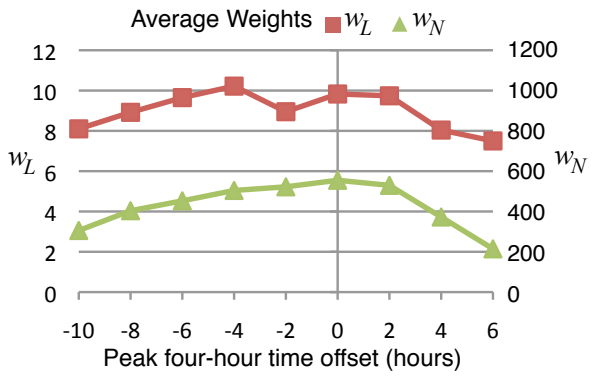

Fig. 5 Dynamic route structure shifted every two hours.

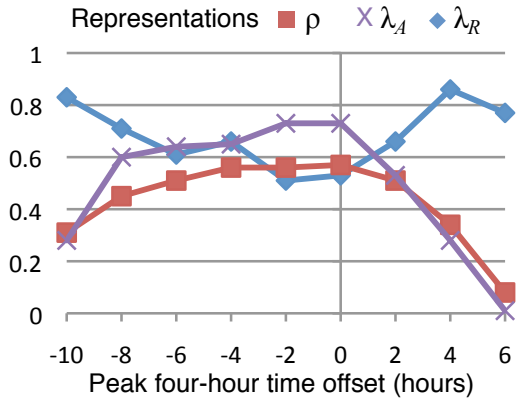

Fig. 6 Dynamic route structure shifted every two hours.

structure representation. Structure deviation metrics are more accurate when representations are high. The δ_A inaccuracies introduced by unrepresented airways are more prominent because the airway structure is stable and covers all of ZKC, whereas the route structure becomes more localized as λ_R decreases. With extremely localized route structures such as at peak+6, unrepresented airway segments in West ZKC introduce large errors because the closest links are far away in East ZKC.

5 User Preferred Routing

This section compares route structures for several different routing options. The same 4/21/2009 flight schedules used to generate filed flight plan

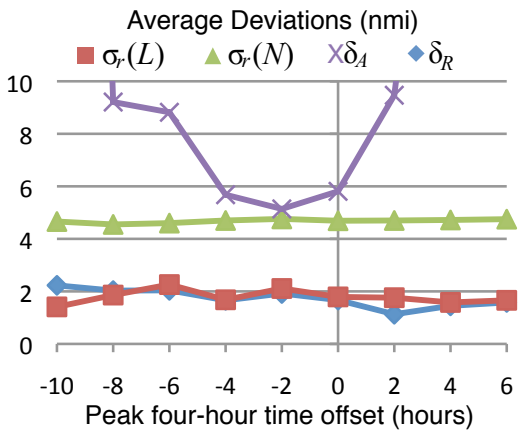

Fig. 7 Dynamic route structure shifted every two hours.

tracks in section 3 were used to generate great circle tracks and weather rerouted tracks for the same peak four-hour time period (15:30-19:30 local) in ZKC.

5.1 Great Circle Routing

The route structure of great circle flight tracks resulted in significantly lower intersection representation than that of flight plan tracks when using parameters from Table 2. When the cluster filtering parameters were reduced to increase intersection representation to a value similar to the flight plan route structure, the number of links and nodes quadrupled with no increase in average link weight and a decease in average node weight. Figure 8 shows great circle route structures with the original parameters on top and reduced cluster filter parameters on the bottom. In addition to increased numbers of links and nodes, Fig. 8 shows how lowering the cluster filters significantly shortened the average link length. This reaffirms the integrity of the originally chosen parameters. The total number of flight pair intersections was actually quite similar between flight plan and great circle routing. Great circle routing simply spread these intersections out more randomly such that only 21% of the traffic intersections were stable enough to form a structure.

Figure 8 also shows how great circle route structure rarely conforms to the airway structure.

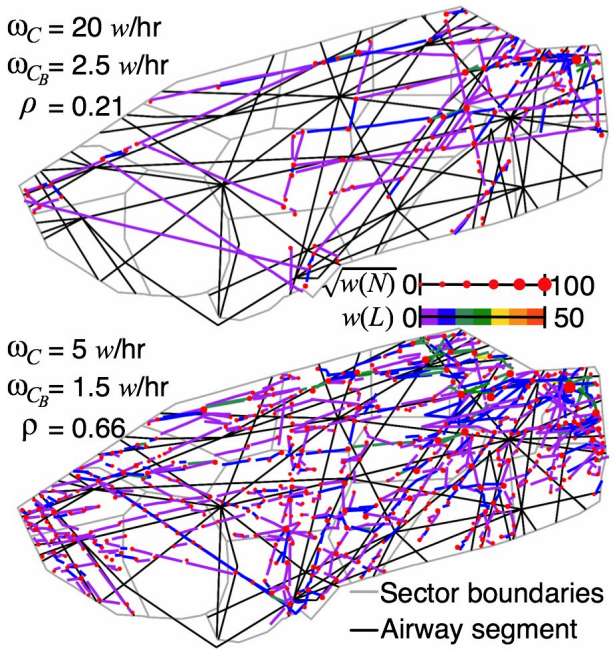

Fig. 8 Great circle route structures for original and reduced cluster filters.

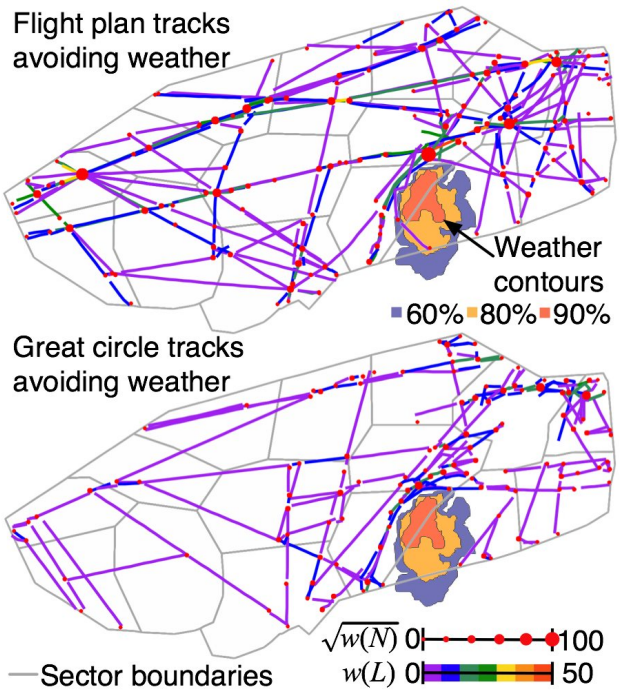

Fig. 9 Route structures for flight plan and great circle tracks avoiding weather.

The largest nodes are in different places than the flight plan route structure and are often close to sector boundaries. If the future airspace system is to support user preferred routing, route structures like these will enable designing airspace to accommodate them.

5.2 Weather Avoidance Reroutes

User preferred reroutes around weather were simulated [9] for both original flight plans and great circle routing. The simulated weather were stationary contours of percent likelihood that a flight would avoid the area [10]. These weather contours blocked several airways in Southeast ZKC.

Figure 9 shows the route structures for the flight plan and great circle tracks avoiding weather. The weather contours are shown underlying the route structure with color indicating the percent likelihood of a flight avoiding the area. Both route structures clearly show links of relatively high weight curving to avoid the weather. In the flight plan based route structure, a new node with weight 10,088 ($\sqrt{w(N)} \approx 100$) appears just north of the weather. This is much larger than the largest weight node ($w(N) = 6,885, \sqrt{w(N)} \approx 83$) from the non weather impacted route structure in Fig. 2. Although the non weather impacted great circle route structure at the top of Fig. 8 does not show any significant structure in the weather location, weather reroutes sufficiently compressed flight tracks to form the structure around the weather seen at the bottom of Fig. 9.

5.3 Comparative Analysis

Route structures were compared between flight plan and great circle tracks and between original and weather rerouted tracks. Figure 10 shows precision metrics for each of these four route structures. As mentioned in section 5.1, ρ is significantly lower for great circle routing and numbers and weights of nodes and links follow a similar trend. The pre-filtered sum weight of all I was actually only 10% less for great circle than flight plan routing, indicating a similar overall complexity in terms of conflict likelihood. How-

ever, great circle routing spread out these intersections such that most were filtered. Weather reroutes actually caused a slight increase in ρ for great circle because of the track compressing effect of the weather obstacle. Route structures had higher $\sigma_r(L)$ for user preferred routing options; $\sigma_r(L)$ was higher for great circle route structures than for flight plan route structures and was higher for route structures with weather reroutes than for routes structure without weather reroutes. In contrast, $\sigma_r(N)$ was far less affected by routing. $\sigma_r(N)$ was slightly greater for weather reroutes than original routing, following a similar although less pronounced trend as $\sigma_r(L)$. However, an opposite trend to $\sigma_r(L)$ appeared in that $\sigma_r(N)$ was slightly less for great circle than flight plan routing.

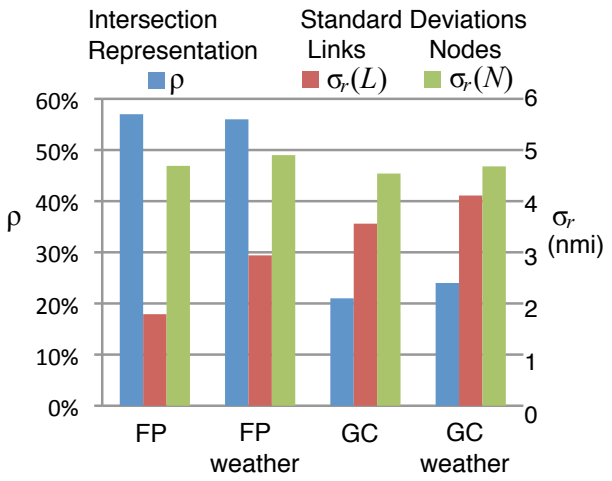

Fig. 10 Precision metrics comparing flight plan (FP) to great circle (GC) and original routing to weather reroutes.

In addition to metrics compared in pervious sections, metrics relating route structure to sector boundaries were compared. Let $\overline{n_L}$ and $\overline{n_N}$ be the average numbers of unique links and interior nodes, respectively, within each sector. Each additional link or node within a sector potentially increases the focus split of a controller. Let $\overline{n_{L_X}}$ be the average number of links entering or exiting a sector. A lower $\overline{n_{L_X}}$ is preferred to minimize sector handoff workload for controllers. Let $\widehat{n_L}$, $\widehat{n_N}$, and $\widehat{n_{L_X}}$ be maximum numbers of links, nodes, and boundary crossing links, respectively, in a single sector. Figure 11 shows these sector relative numbers of links and nodes. The total numbers of links and nodes were less for great circle than flight plan route structure but greater for weather reroutes than original routes. The averages in Fig. 11 echo this result. The increased averages can be attributed to weather reroutes that cause flights to fly through a few extra sectors to avoid the weather. Even though the average number of links per sector was less for great circle than flight plan route structure, the maximum number of links was greater due to the shifting location of links with respect to sector boundaries. The same effect is seen for maximum nodes for weather rerouted great circle tracks.

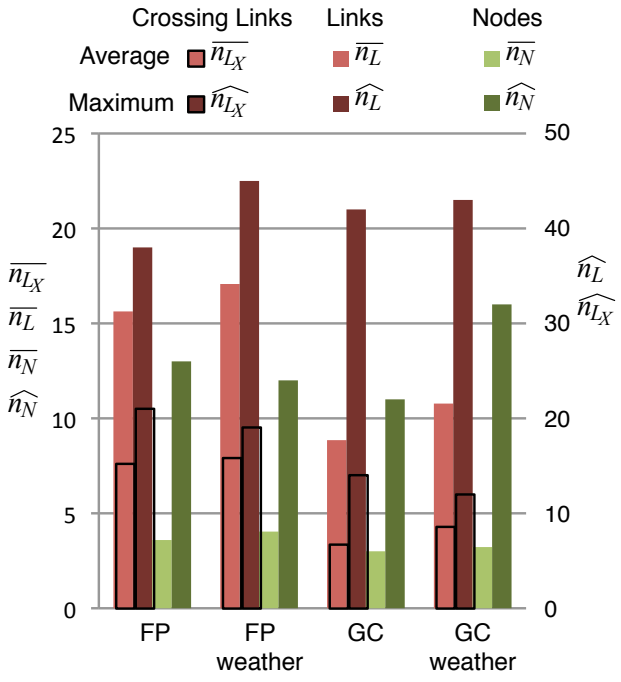

Fig. 11 Average and maximum links and nodes per sector.

Controllers prefer major flows and critical points to be well within sector boundaries. Controllers must be aware of not only flights within a sector, but also just outside the sector boundary to guarantee separation. Ideally flows should stay at least five nmi inside the sector boundary to avoid magnifying flight awareness workload of neighboring sectors. Controllers require some time to

become familiar with a flight entering the sector before it approaches a critical point. The more time they have, the more efficiently they may control the flow safely through the critical point. Therefore, the length of flow segments from the point they enter a sector to when they encounter a critical point should be maximized. Let η_{L_n} be the percent of points along link nominal paths that are within five nmi of a sector boundary. Let η_{N_n} be the percent of nodes that serve as the end point of a link entering a sector within 10 nmi. Let η_{L_w} and η_{N_w} be η_{L_n} and η_{N_n} percentages normalized by link and node weights. Figure 12 shows these percentages of link and node sector boundary proximity. η_{L_n} and η_{L_w} do not change significantly with weather reroutes but they do increase noticeably from flight plan to great circle routing. Great circle routing affects the location of links to be more random with respect to sector boundaries. η_{N_n} decreases from flight plan to great circle routing due to the significant reduction total number of nodes. However, the increase in η_{N_w} from flight plan to great circle routing shows how the traffic randomizing affect of great circle routing moved some larger nodes too close to sector boundaries. This effect is amplified in the great circle weather reroutes.

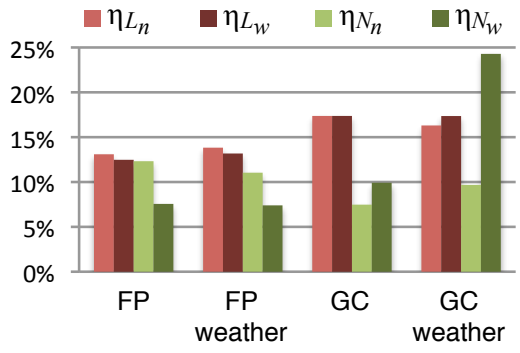

Fig. 12 Percentages of links and nodes close to sector boundaries.

6 Conclusion

This paper presented a method of defining route structure from a given set of flight tracks. A parametric analysis identified optimal method parameters to define good weather route structures similar to today's published airway structure. Flight tracks simulated from four different days of flight schedules were tested with similar results compared to the airway structure. On average, the route structures deviated only 1.7 nmi from airways.

Route structures were generated for four-hour time windows of track data shifted every two hours to demonstrate how route structure can be updated dynamically. Links and nodes of the route structure appeared and increased in weight as flight traffic increased. When airways began to saturate, more and more links began to appear where airways had not been published, but the precision of the route structure in representing the track data remained stable. On average, the standard deviation of flights tracks was 2 nmi from links and 4.7 nmi from nodes.

Route structures of great circle routing differed significantly from flight plan routing. Great circle tracks displayed much less structure with lower traffic intersection representation and link and node weights than flight plan tracks. However, great circle route structure had larger average numbers of links and nodes per sector than flight plans, as well as a higher percentage of the route structure close to sector boundaries. Simulated user preferred reroutes around a stationary weather obstacle produced route structures with greater numbers of link sector boundary crossings and average links and nodes per sector. Weather reroutes of great circle tracks resulted in a significant increase in larger weight nodes close to sector boundaries. These results demonstrate how dynamically generated route structures could be useful in guiding dynamic airspace configuration to accommodate traffic volume changes or weather reroutes. They also suggest that while route structure may help controllers retain situational awareness under dynamically changing traffic conditions, it may not help in traffic with little structure such as with great circle routing.

References

[1] Histon, J.M., Hansman, R.J., Aigoin, G., Delahaye, D. and Puechmorel, S. (2002) "Introducing structural considerations into complexity metrics," *Air Traffic Control Quarterly*, Vol. 10, No. 2, pp. 115-130.

[2] Sabhnani, G. R., "Geometric algorithms for dynamic airspace sectorization," Ph.D. thesis, Stony Brook University, NY, May 2009.

[3] Xue, M. "Three dimensional sector design with optimal number of sectors," *AIAA Guidance, Navigation, and Control Conference and Exhibit*, Toronto, Ontario, Canada, August 2010.

[4] Martinez, S., Chatterji, G., Sun, D., Bayen, A. "A weighted-graph approach for dynamic airspace configuration," *AIAA Guidance, Navigation, and Control Conference and Exhibit*, Hilton Head, South Carolina, August 2007, AIAA-2007-6448.

[5] Li, J., Wang, T., and Hwang, I. "A spectral clustering based algorithm for dynamic airspace configuration," *9th AIAA Aviation Technology, Integration and Operations Conference*, Hilton Head, South Carolina, September 2009, AIAA-2009-7056.

[6] Sridhar, B. and Sheth, K. "Network Characteristics of Air Traffic in the Continental United States," *Proceedings of the 17th International Federation of Automatic Control World Congress*, Coex, South Korea, 2008.

[7] Sabhnani, G., A. Yousefi, D.P. Kierstead, I. Kostitsyna, J.S.B. Mitchell, and V. Polishchuk, "Algorithmic traffic abstraction and its application to NextGen generic airspace," *10th AIAA Aviation Technology, Integration, and Operations Conference*, Fort Worth, Texas, September 2010.

[8] Zelinski, S. "Defining critical points for dynamic airspace configuration," *26th International Congress of the Aeronautical Sciences*, Anchorage, Alaska, 2008.

[9] Love, J., Chan, W., and Lee, C.H. "Analysis of Automatetd Aircraft Conflict Resolution and Weather Avoidance," *9th AIAA Aviation Technology, Integration and Operations Conference*, Hilton Head, South Carolina, September 2009, AIAA-2009-6995.

[10] DeLaura, R., and Evans, J., "An Exploratory Study of Modeling En Route Pilot Convective Storm Flight Deviation Behavior," *Proceedings of the 12th Conference on Aviation, Range, and Aerospace Meteorology*, Atlanta, Georgia, 2006.

6.1 Copyright Statement